Anal Bioanal Chem (2011) 401:1231–1239
DOI 10.1007/s00216-011-5203-0

ORIGINAL PAPER

Combined Raman and IR spectroscopic study on the radical-based modifications of methionine

A. Torreggiani · S. Barata-Vallejo · C. Chatgilialoglu

Received: 10 May 2011 / Revised: 21 June 2011 / Accepted: 21 June 2011 / Published online: 15 July 2011

Abstract Among damages reported to occur on proteins, radical-based changes of methionine (Met) residues are one of the most important convalent post-translational modifications. The combined application of Raman and infrared (IR) spectroscopies for the characterisation of the radical-induced modifications of Met is described here. Gamma-irradiation was used to simulate the endogenous formation of reactive species such as hydrogen atoms ($^{\bullet}H$), hydroxyl radicals ($^{\bullet}OH$) and hydrogen peroxide (H_2O_2). These spectroscopic techniques coupled to mass experiments are suitable tools in detecting almost all the main radical-induced degradation products of Met that depend on the nature of the reactive species. In particular, Raman spectroscopy is useful in revealing the radical-induced modifications in the sulphur-containing moiety, whereas the IR spectra allow decarboxylation and deamination processes to be detected, as well as the formation of other degradation products. Thus, some band patterns useful for building a library of spectra–structure correlation for radical-based degradation of Met were identified. In particular, the bands due to the formation of methionine sulfoxide, the main oxidation product of Met, have been identified. All together, these results combine to produce a set of spectroscopic markers of the main processes occurring as a consequence of radical stress exposure, which can be used in a spectroscopic protocol for providing a first assessment of Met modifications in more complex systems such as peptides and proteins, and monitoring their impact on protein structure.

Keywords Methionine · Radical stress · Raman spectroscopy · IR spectroscopy · Gamma-radiolysis

Abbreviations

Aba	α-Aminobutyric acid
ESI	Electron spray ionisation
GC/MS	Gas chromatography/mass spectrometry
HomoSer	Homoserine
IR	Infrared
Met	Methionine
Met(O)	Methionine sulfoxide
MTPA	3-(Methylthio)-propionaldeide
$MTPNH_2$	3-(Methylthio)-propionamine

Introduction

The amino acid sequence in a protein is a reflection of the DNA sequence of the corresponding gene and ultimately establishes the function of the protein, whether it be structural or catalytic. However, it is also well established that post-translational modification of proteins can markedly affect biological activity. Among the covalent post-translational modifications, oxidation of methionine residues is one of the most important consequences of the attack of reactive oxygen species (ROS) [1, 2]. This is

Electronic supplementary material The online version of this article (doi:10.1007/s00216-011-5203-0) contains supplementary material, which is available to authorized users.

A. Torreggiani (✉) · S. Barata-Vallejo · C. Chatgilialoglu
I.S.O.F., Consiglio Nazionale delle Ricerche,
Via P. Gobetti 101,
40129 Bologna, Italy
e-mail: torreggiani@isof.cnr.it

S. Barata-Vallejo
Faculty of Pharmacy and Biochemistry,
University of Buenos Aires,
1053 Buenos Aires, Argentina

illustrated by Reaction 1 where hydrogen peroxide (H_2O_2) is used as ROS.

$$\text{Met} + H_2O_2 \rightarrow \text{Met(O)} + H_2O \quad (1)$$

The methionine residues in a number of proteins and peptides including *Escherichia coli* ribosomal protein L12, α-chymotrypsin and adrenocorticotropin have been oxidized in this fashion [3, 4]. The presence of methionine sulfoxide (Met(O)) residues can lead to severe effects on protein structure and function. For example, oxidation of Met to Met(O) destroys the antiproteinase activity in α-antitrypsin [5], can lead to significantly shorter half-lives of human IgG monoclonal antibodies and has important repercussions for calcium/calmodulin signalling, since oxidation-induced unfolding/structural destabilization takes place [6, 7].

Unlike the oxidation of all other amino acid residues (except cysteine residues), the oxidation of Met residue can be reversed by the action of an enzyme methionine sulfoxide reductase (Mrs). For this reason, it has been hypothesized that Met residues could function as a "last chance" antioxidant defence system for proteins [8]. In fact, as endogenous components of proteins, their effective concentration is very high, providing effective scavenging of oxidants before they can attack residues that are critical to structure or function [8, 9].

Although Met(O) can be "repaired", oxidatively modified forms of Met residues accumulate in living systems, also due to the impairment of the turnover and defence systems; this is involved in a number of degenerative process during aging and pathological conditions. Thus, establishing approaches that allow detection of Met modifications in proteins at early stages can be of great importance for assessment and monitoring its impact on protein structure.

The oxidation of Met occurs either by non-radical oxidants (like H_2O_2, HOONO or HOCl) or by radical species [10–12]. Although the non-radical oxidation is site-specific with the formation of Met(O), the radical-based oxidation is more complex [13]. Recently, the reaction mechanisms of reactive species such as $HO^{\bullet}$ and $H^{\bullet}$ (generated by gamma-radiolysis) with free Met have been elucidated in the absence and presence of molecular oxygen [14]. Based on detailed product studies, it has been found that the major product of $HO^{\bullet}$ radical attack in the absence of molecular oxygen is the α-aminoalkyl radical that can be converted into the corresponding amine ($MTPNH_2$) and aldehyde (MTPA) derivatives (Scheme 1). The latter becomes the major product of $HO^{\bullet}$ radical attack in the presence of molecular oxygen. As regards $H^{\bullet}$ atoms attack, the major products are α-aminobutyric acid (Aba) or homoserine (HomoSer), depending on the absence or presence of oxygen,

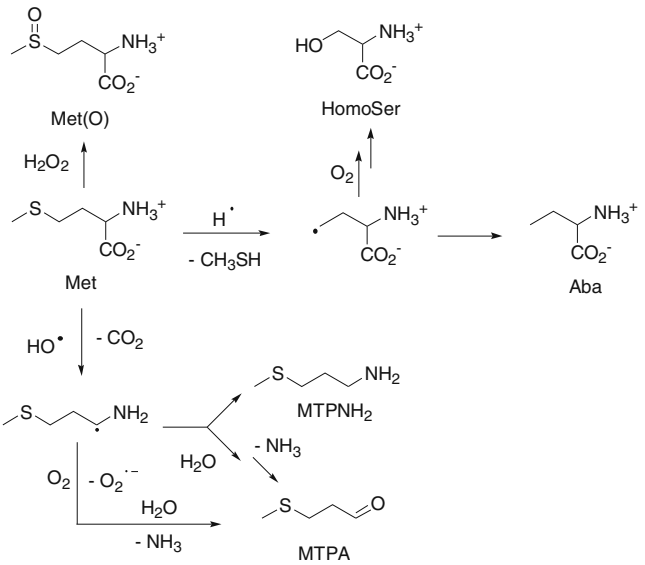

Scheme 1 Reaction mechanisms for the γ-irradiation of N_2O-saturated Met solutions in the absence and presence of oxygen

respectively. On the contrary, Met(O) has resulted only from the oxidation action of H_2O_2 [14].

To obtain information on the radical-induced products of individual amino acids or small peptides, gas chromatography/mass spectrometry (GC/MS) and electron spray ionisation (ESI)-Ion Trap MS have been generally used. MS analysis is particularly informative given the wealth of structural information that can be obtained from fragmentation patterns and its ability to screen for multiple products (if their masses are known or can be predicted) in single runs [15].

In this context, vibrational spectroscopy can give a useful contribution since it is capable of providing a rapid and non-destructive analysis of the samples. Combined with their little or no requirement for sample preparation, infrared (IR) and Raman spectroscopies can be good analytical methods for detection of Met modifications and assessment of their effects on proteins.

The aim of the present study is the detection of Raman and IR band patterns useful for building a library of spectra–structure correlations for radical-based degradation of Met. Model stress conditions were obtained by using γ-radiolysis of aqueous solutions as source of free radicals, and different experimental conditions were considered in order to obtain a selection of the reacting radical species. In radiolysis of water, together with radical ($HO^{\bullet}$) and non-radical oxidants (H_2O_2), primary reducing species like hydrated electrons (e_{aq}^-) and $H^{\bullet}$ atoms are produced. The reaction of the latter reducing species with sulfur-containing residues in proteins has been recently studied in connection with tandem protein/lipid damages [16–18].

Raman and IR techniques coupled to mass experiments have shown to be suitable tools in detecting almost all the

main radical-induced degradation products of Met. In particular, some markers bands, potential useful for detecting the main oxidation products of Met in more complex systems such as proteins, were identified.

Experimental

Materials

The following commercially available starting materials were obtained from Sigma-Aldrich Co. and used as received: L-methionine (Met), L-homoserine (HomoSer), L-methionine-(R,S)-sulfoxide (Met(O)), L-2-aminobutiric acid (Aba), 3-(methyl-thio)-propionamine ($MTPNH_2$) and 3-(methyl-thio)-propionaldeide (MTPA). Solvents were purchased from Merck (HPLC grade) and used without further purification. Water was purified with a Millipore system. All aqueous amino acid solutions were prepared immediately before use.

Methods

Continuous radiolysis was performed on Met aqueous solutions containing by using a ^{60}Co-Gammacell at the dose rate of ~6.5 Gy/min. The exact absorbed radiation dose was determined with the Fricke chemical dosimeter, by taking $G(Fe^{3+})=1.61$ μmol J^{-1} [19]. Mixtures of gases were obtained by an appropriate mixing, controlled by flow meter. The gas stream was obtained by a line connected with a needle inserted in the vessel, and the flow was adjusted to get a continuous bubbling during irradiation. Met solutions (10 mM) were freshly prepared at natural pH (5.8) in tri-distilled water. Aliquots of the solutions were transferred in different vials and saturated with N_2O or N_2O/O_2. One of the vials was directly lyophilised, whereas the other vials were irradiated at 4 kGy dose and then lyophilised.

When diluted aqueous solutions are irradiated, practically all the energy absorbed is deposited in water molecules, and the chemical changes in solutes are brought about indirectly by the primary water reactive species that are three short-lived species, hydrated electron (e_{aq}^-), hydroxyl radicals ($^{\bullet}OH$) and hydrogen atoms ($H^{\bullet}$), together with H^+ and H_2O_2 that make start the reaction sequence (Eq. 2) [20, 21].

$$H_2O \xrightarrow{\gamma} e_{aq}^-(0.27), HO^{\bullet}(0.28), H^{\bullet}(0.06), H^+(0.27), H_2O_2(0.07) \quad (2)$$

The values in parentheses represent the radiation chemical yields (G) in units of micromoles per Joule. Radical stress on Met was stimulated in the absence and presence of oxygen. In N_2O saturated solutions (~0.02 M of N_2O), e_{aq}^- are efficiently transformed into $HO^{\bullet}$ radicals [Eq. 3, $k_3=9.1\times10^9$ M^{-1} s^{-1}], affording a $G(HO^{\bullet})=0.55$ μmol J^{-1}, i.e. $H^{\bullet}$, H_2O_2 and $HO^{\bullet}$ species accounted for 9%, 9% and ~82%, respectively, of the reactive species. This condition has been used as model of oxidative damages occurring in vivo [22, 23], where $^{\bullet}OH$ radicals play a prominent role; this model is also used for making biochemical correlations with human diseases and ageing [24].

$$e_{aq}^- + N_2O + H_2O \rightarrow HO^{\bullet} + N_2 + HO^- \quad (3)$$

Under N_2O/O_2 (90/10, *v*/*v*) saturation, e_{aq}^- are still efficiently converted into $HO^{\bullet}$ (Eq. 3) that remain the main radical species formed in the system. On the contrary, $H^{\bullet}$ radicals (~10% of the total radical species formed) are portioned between oxygen and Met: 20% of $H^{\bullet}$ are transformed into $O_2^{-\bullet}$ (Eqs. 4 and 5) and 80% react with Met. As regards $HO_2^{\bullet}/O_2^{-\bullet}$, they give rise to a disproportionation reaction, leading to H_2O_2 production (Eq. 6). Thus, under these conditions, the H_2O_2 concentration is higher than in the absence of oxygen.

$$H^{\bullet} + O_2 \rightarrow HOO^{\bullet} \quad (4)$$

$$HOO^{\bullet} \rightleftharpoons O_2^{-\bullet} + H^+ \quad (5)$$

$$O_2^{-\bullet} + HO_2^{\bullet} + H_2O \rightarrow H_2O_2 + O_2 + HO^- \quad (6)$$

The Raman spectra were recorded by a Bruker IFS 66 spectrometer equipped with a FRA-106 Raman module and a cooled Ge-diode detector. The excitation source was a Nd^{3+}-YAG laser (1,064 nm), the spectral resolution was 4 cm^{-1} and the total number of scans for each spectrum was 800. The laser power on the sample was about 100 mW. No carbonization effect was observed on the focused part of the samples.

The IR spectra were recorded by using a Nicolet 5700 FT-IR/ATR (64 scans; resolution, 4 cm^{-1}) on diamond crystal. Raman and IR spectra were obtained on lyophilized samples in order to improve the signal/noise ratio. Lyophilisation was performed on a Modulyo 4K Freeze Dryer equipped with a RV8 Rotary Vane Pump (Edwards).

Structural information were also obtained from multiple fragmentation experiments using ESI-Ion Trap MS^n on an Esquire 3000 Plus mass spectrometer (Bruker Daltonics) equipped with a Cole Parmer syringe pump. All sample solutions were prepared in 0.1% formic acid in water. The measurements were performed for two types of samples: (a) 1×10^{-5} mol L^{-1} standard solutions of Met, HomoSer, Met (O), Aba or $MTPNH_2$ and (b) 1/100 dilutions of the irradiated Met solutions under N_2O saturated conditions or

continuously flushed with N_2O/O_2 (90/10) during the irradiation time. The samples were infused at a flow rate of 400 μL min^{-1}. The analyses were performed in positive mode, the nebulizer pressure was 30 psi, the drying gas flow was 10 L min^{-1} and the drying gas temperature was 365 °C.

GC/MS measurements were performed by a Finnigan Mat GCQ. Analyses were obtained on a 30-m×0.25-mm×0.25-μm cross-linked (5% phenyl)-methylpolysiloxane capillary column (DB-5). Oven program was as follows: starting at 30 °C for 5 min, followed by an increase of 5 °C up to 250 °C. The analyses were performed on a $CHCl_3$ extract of the irradiated samples and on a $CHCl_3$ solution of 3-methylthiopropanaldehyde reference compound.

Results and discussion

Characterisation of Met-irradiated solutions

The samples prepared for this study were analysed by spectroscopic and spectrometric approaches described in the "Experimental" section. ESI-Ion Trap MS^n and GC/MS measurements were performed to verify the formation of the Met degradation products, previously identified, in the absence of oxygen and presence of oxygen (Scheme 1) [14]. The irradiated solutions were analyzed by direct infusion ESI-MS, whereas a $CHCl_3$ extract of the irradiated samples was obtained to be analyzed by GC/MS.

Figure 1a shows the ESI-MS analysis of crude reactive mixture N_2O-saturated Met sample after 4 kGy irradiation dose. The MS^1 spectrum confirmed the presence of 3-methylthiopropylamine ($MTPNH_2$) [*m/z* 106.2 ($MTPNH_2+H^+$)], the starting material [*m/z* 150.2 (Met + H^+) and 172.4 (Met + Na^+)] and Met sulfoxide (Met(O)) [*m/z* 166.3 (Met(O) + H^+) and 188.3 (Met(O) + Na^+)]. In addition, to verify the presence of 2-aminobutiric acid (Aba), the product caused by the desulfuration reaction leading also to the production of CH_3SH (Scheme 1), the ion with *m/z*=104.0 (Aba + H^+) was isolated. The MS^2 spectrum showed a daughter ion with *m/z*=58.0 due to the loss of $CO+H_2O$ from Aba (Fig. 1b) [25]. The MS^2 spectra were taken also for the ions corresponding to Met(O) and $MTPNH_2$, further confirming the peak assignments (see Figs. S1 and S2 in Electronic Supplementary Material). The spectra recorded for the irradiated sample were compared with those obtained from the standard solutions analyses.

Analogously, the ESI-MS analysis was performed on the irradiated Met sample continuously flushed with N_2O/O_2 (90/10) during the irradiation time. The determination revealed the presence of Met [*m/z* 150.2 (Met + H^+) and *m/z* 172.1 (Met + Na^+)] and Met(O) [*m/z* 166.2 (Met(O) + H^+) and *m/z* 188.1 (Met(O) + Na^+)] (Fig. 2a). Also, the formation of HomoSer in the reaction mixture was confirmed by isolating the ion *m/z*=120 (Homoser + H^+) (Fig. 2b). In fact, the MS/MS spectra showed the formation of the ions *m/z* 101.9 (HomoSer−H_2O), *m/z* 74.2 (HomoSer – ($CO+H_2O$)) and *m/z* 56.0 due to the loss of water from the immonium ion formed during the ionization process [25]. The spectra recorded on the irradiated sample were compared with those obtained from the standard solutions analyses. Also, in this case, the MS recorded spectra were identical to those obtained for the reference compounds.

In addition, the presence of the 3-methylthiopropanaldehyde (MTPA) was confirmed by GC/MS analyses of a $CHCl_3$ extract of the irradiated samples both in the absence and presence of O_2, followed by spike experiments. In all cases, a peak with retention time of 3.54 min was obtained (see Electronic Supplementary Material Fig. S3).

Degradation of Met in deareated aqueous solutions

To gain information on the spectra–structure correlations, the vibrational spectra were recorded. The Raman spectra of Met before and after irradiation under N_2O saturation are provided in Fig. 3, and the tentative assignments of the main bands are listed in Table 1. Under these conditions, $HO^\bullet$ (mainly), $H^\bullet$ and H_2O_2 are the reactive species attacking Met residue.

From a qualitative examination of the spectra, many differences were evident, in particular, in the bands due to sulfur-containing moiety and the CH_2 group.

The side group $–C^\beta H_2C^\gamma H_2–S^\delta–CH_3$ can assume different molecular forms in solution. The side chain of Met is indeed more flexible than the side chains of leucine or isoleucine, residues of comparable low polarity, and this flexibility depends more on the presence of the sulfur atom than on the lack of branching [26]. The C–S stretching modes of this group can give rise to three bands of which the ~720-cm^{-1} band has been attributed to the *trans* form, the ~700-cm^{-1} to the *gauche* form and the ~655-cm^{-1} to both [27]. In the present investigation, strong Raman bands at 723 (the most intense), 701 and 657 cm^{-1} were visible in the spectrum of Met (Fig. 3a). This confirms that untreated Met is manly in the *trans* position with respect to the $–C^\gamma–S^\delta$, which is in good agreement with the X-ray investigation [27]. Radical stress exposure induced a change in the population ratio of the two molecular forms as shown by the significant decrease in the doublet intensity (I_{721}/I_{701}; Fig. 3b). The νC–S bands were also visible in the IR spectra (at 720 and 708 cm^{-1}), although their intensities were very low (Fig. 4).

The radical-based degradation of Met caused a complete inversion of the intensity ratio of the Raman double at 1,445 and 1,424 cm^{-1}, due to the in-plane deformation of

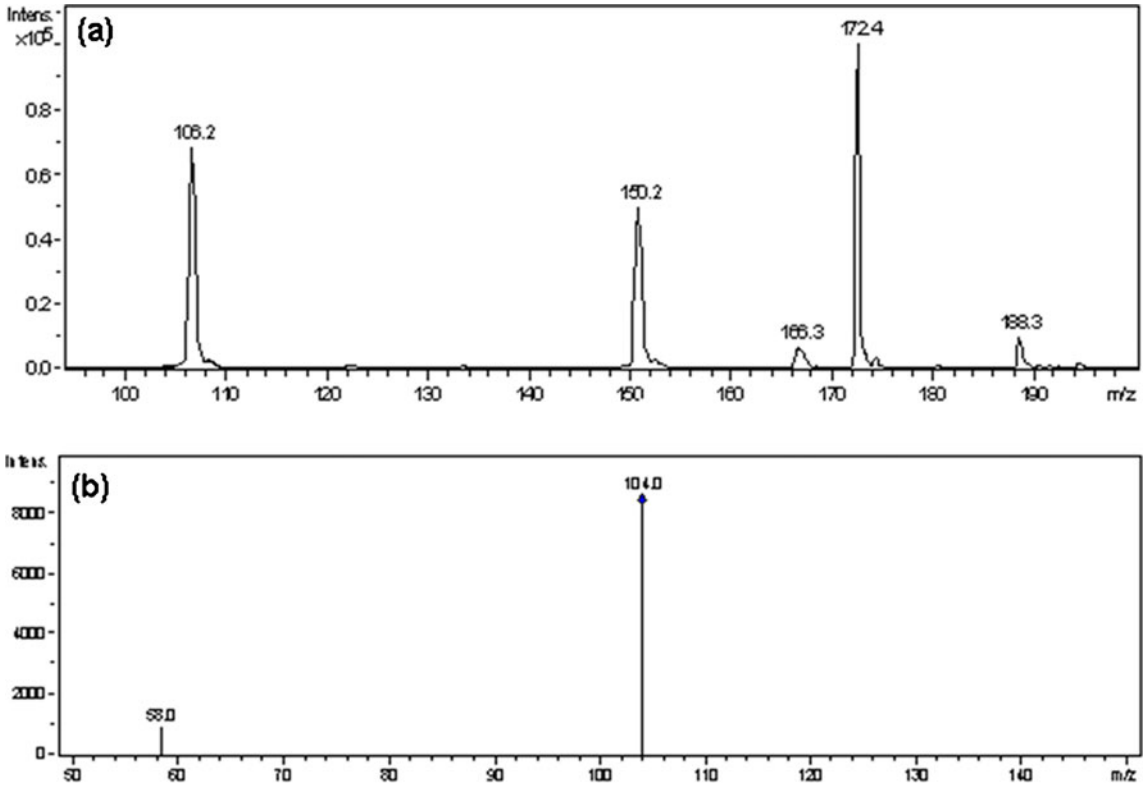

Fig. 1 **a** ESI-Ion Trap MS^1 spectrum of 10 mM irradiated Met sample saturated with N_2O. **b** ESI-Ion Trap MS^2 of the daughter ion with m/z=104 (Aba + H^+)

–CH_3 and –CH_2 groups (Fig. 3a, b) [28, 29]. This spectral changes can be connected with the modifications in the structure of the aliphatic chain and in the number of the CH_2 groups that take place both because of the desulfurisation reaction caused by the $H^•$ attach on the sulfur atom of Met, and the decarboxylation process due to the $HO^•$ attack: the first leads to the formation of CH_3SH and the second to the corresponding amine and aldehyde (Scheme 1) [18, 30–34]. The change in the CH_2 moieties was particularly evident in the difference spectrum (Fig. 3c), obtained by subtracting from the untreated Met spectrum that of irradiated Met: the $\delta CH_2/\delta CH_3$ band was well visible at about 1,446 cm^{-1}, as well as other bands due to some CH_2 deformations (i.e. 1,352, 1,322, 878 and 764 cm^{-1}) [28], indicating relevant modifications in the methylene structure and content before and after stress exposure. This result was further supported by the weak intensity change of the Raman band at 2,856 cm^{-1} due to the C–H stretching modes of CH_2 groups, as well as by the IR bands at 2,920 and 2,850 cm^{-1}, visible in the difference spectrum (Fig. 5B (a)) [35]. Taking into account that $G(HO^•)+G(H^•)+G(H_2O_2)=0.68$ μmol J^{-1}, these spectral changes are so evident in the vibrational spectra since about 90% of the reactive species $(G(HO^•)+G(H^•)=0.61$ μmol $J^{-1})$ results to affect the aliphatic backbone of Met (Scheme 1).

In agreement with the decarboxylation reaction expected to occur as a consequence of the $^•OH$ radical attack on Met (Scheme 1), changes in the bands due to the carboxylate group vibrations were visible. In particular, an intensity decrease in the shoulder at 1,414 cm^{-1}, due to the COO^- symmetric stretching, as well as in the Raman band at 542 cm^{-1}, due to the COO^- rocking, occurred after irradiation (Fig. 3b and Table 1) [29, 36]. These changes were particularly evident in the difference spectrum, where at least four bands due to the carboxylate group vibrations were clearly visible (Fig. 3c, bands marked by asterisk), indicating a higher content of this functional group in the sample before irradiation. Also in the IR spectrum, the intensity decrease of some COO^- bands was visible, in particular, in the bands at 1,563 ($\nu_a COO^-$), 682 (ωCOO^-) and 645 cm^{-1} (δO–C = O; Fig. 4a, b) [28, 37].

As a consequence of the decarboxylation reaction, also the ionic interactions resulted to be perturbed by the radical attack, as shown by the spectral modifications visible in the 1,580–1,640-cm^{-1} region, where both $–NH_3^+$ and $–COO^-$ groups mainly contribute (Figs. 3 and 4) [28, 38]. In addition, a higher content of NH_3^+ groups is present before radical attack as evidenced by the IR measurements (Fig. 5A) and, in particular, by the difference spectrum where a band at about 3,150 cm^{-1} (νNH_3^+) was clearly visible (Fig. 5B). This can be connected with the formation

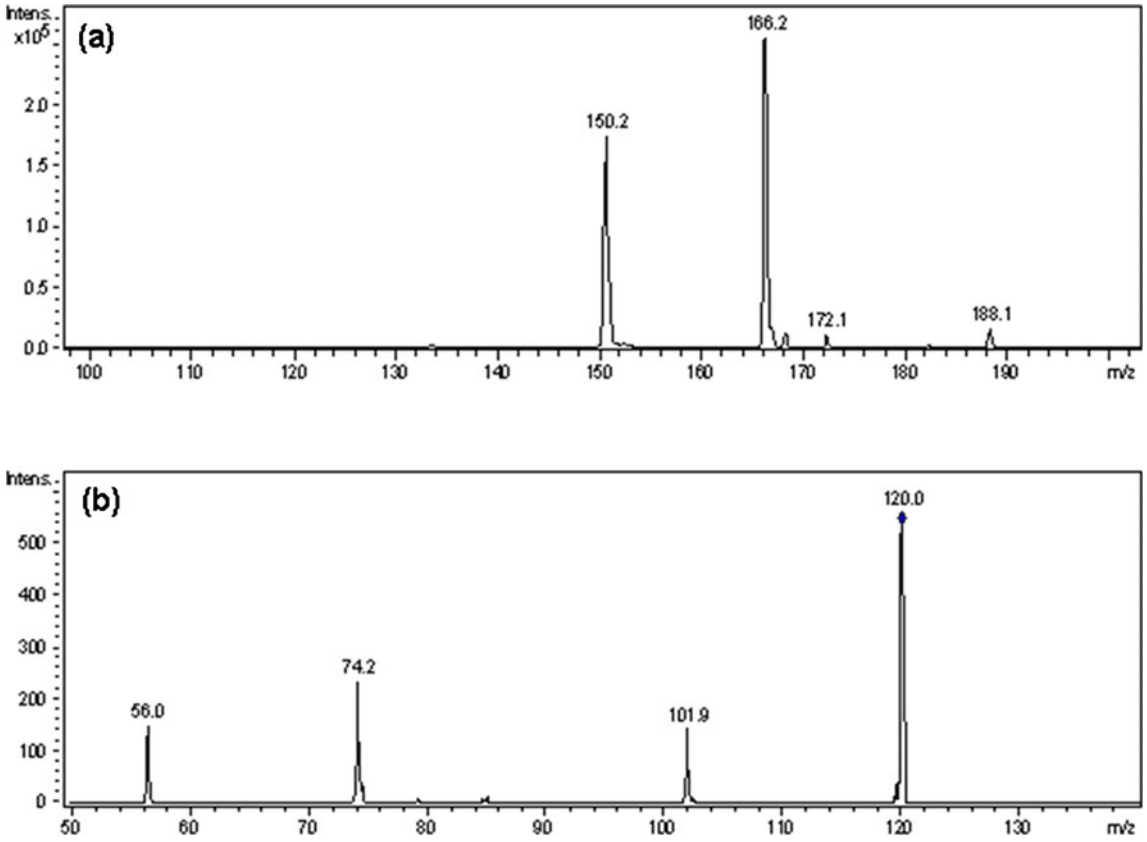

Fig. 2 **a** ESI-Ion Trap MS^1 spectrum of 10 mM irradiated Met sample continuously flushed with N_2O/O_2 (90/10) during γ-irradiation. **b** ESI-Ion Trap MS^2 of the daughter ion with m/z=120 (HomoSer + H^+)

of Met degradation products due to the deamination reactions (Scheme 1).

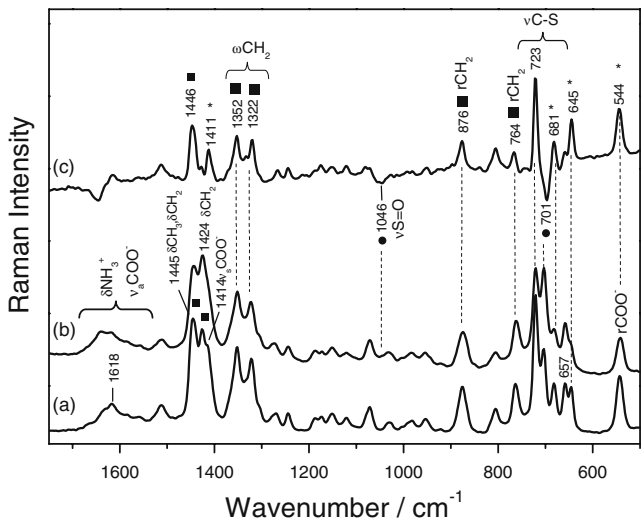

Fig. 3 The 1,750–500-cm^{-1} Raman region of Met (**a**) before and (**b**) after 4 kGy irradiation under N_2O saturation; **c** difference spectrum obtained by subtracting the spectrum of Met irradiated from untreated Met (**a**, **b**). *Asterisks*, *squares* and *circles*: marker bands of changes involving COO^-, CH_2/CH_3 and S-containing moiety, respectively

As regards the negative bands visible in the difference Raman spectrum (Fig. 3c), they are attributable to the formation of new compounds with a different functional group. For example, the broad band about 1,040 cm^{-1}, attributable to the νS = O vibration [26],coupled with the other negative peak at 701 cm^{-1} due to νC–S [34], is indicative of the formation of a small amount of Met(O) due to the reaction of Met with H_2O_2 (Scheme 1) produced from the radiolysis of water (under these conditions, H_2O_2 is about 9% of the total reactive species present in the system) [14]. Thus, the presence of these two bands (marked by circles in Fig. 3) can be considered a marker pattern of this Met oxidation product.

Degradation of Met in oxygenated aqueous solutions

When Met is undergone to radical stress in the presence of oxygen, the formation of the corresponding sulfoxide (Met (O)) is more favoured than in N_2O saturated solution. This conclusion can be drawn out from the analysis of the Raman bands at about 1,040 and 700 cm^{-1} (Fig. 6) that showed a more significant increase in intensity under these experimental conditions than in the absence of oxygen (Fig. 3). In addition, the presence of a more relevant

Table 1 Tentative assignment of the main bands in the Raman spectra of Met before and after irradiation exposure in the absence and presence of oxygen

Raman wavenumbers/cm^{-1}			Assignments
Met untreated	Met irradiated under N_2O	Met irradiated under N_2O/O_2	
542 m	544 m	544 m	$rCOO^-$ (asterisk)
645 m	647 sh,w	649 sh,w	δO–C = O (asterisk)
657 m	657 m	658 m	νC–S (t + g)
681 m	681 sh,m	682 sh,m	ωCOO^- (asterisk)
701 m	701 s	702 vs	νC–S (g) (circle)
723 vs	723 s	723 s	νC–S (t)
764 m	764 m	762 m	rCH_2
806 m	806 w	807 w	νC–C
876 m	876 m	874 m	rCH_2
1,030 w	1,030 w	1,032 w	νC–C–N
–	1,043 sh,w	1,038 w	νS = O (circle)
1,073 m	1,073 m	1,072 m	νC–N
1,152 w	1,152 w	1,152 w	rNH_3^+
1,245 w	1,245 vw	1,246 vw	tCH_2
1,322 s	1,322m	1,322 m	ωCH_2
1,352 s	1,352 m	1,352 m	ωCH_2
1,414 sh,s	–	–	$\nu_s COO^-$ (asterisk)
1,424 s	1,424 vs	1,424 vs	δCH_2 (square)
1,445 vs	1,445 s	1,445 s	δCH_3, δCH_2 (square)
1,590 w	1,590 sh,w	1,588 sh,w	$\nu_a COO^-$, δNH_3^+
1,618 br,w	1,618 br,vw	1,629 br,w	δNH_3^+
–	–	1,679 sh,vw	νHC = O

Assignments: ν stretching, δ in-plane bending, γ out-of-plane bending, *t* twisting, *r* rocking, ω wagging. Intensities: *w* weak, *m* medium, *s* strong, *v* very, *sh* shoulder, *br* broad

Asterisk, *circle*, *square* marker bands useful for identifying changes in COO^-, CH_2/CH_3 and sulfur-containing moieties

amount of the sulfoxide derivative was further confirmed by the difference IR spectra (Fig. 7). In fact, two bands at about 1,037 and 1,020 cm^{-1}, due to the νS = O differently H-bonded, were visible under both conditions. The intensity of the latter was stronger in the presence of oxygen

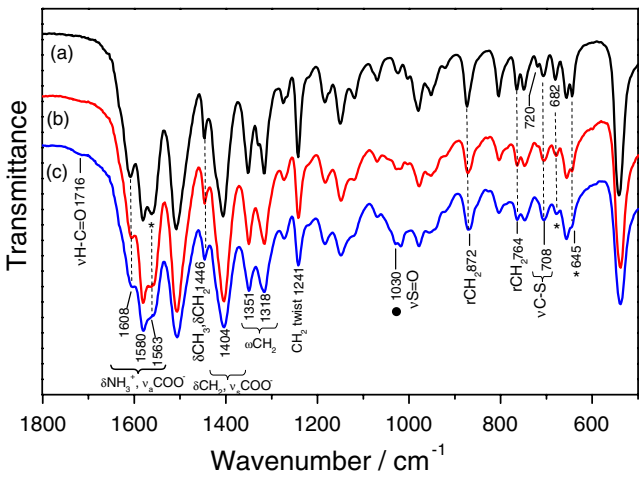

Fig. 4 The 1,800–500 cm^{-1} IR region of Met (**a**) before and after 4 kGy irradiation under N_2O (**b**) or N_2O/O_2 (90/10) (**c**) saturation. *Asterisks* and *circles*: marker bands of changes involving COO^- and S-containing moiety, respectively

(Fig. 7b), indicating a higher degree of Met oxidation, as expected since under these conditions, the H_2O_2 concentration is higher than in the absence of oxygen (Eqs. 4–6). In accordance with this result, a larger amount of Met was degradated under N_2O/O_2 atmosphere, as indicated by the more relevant intensity decrease in the I_{723}/I_{700} doublet (~55% and ~40% under N_2O/O_2 and N_2O saturation, respectively; Figs. 6 and 3).

As observed in the absence of oxygen, the intensity of the doublet at 1,445 and 1,427 cm^{-1} underwent a complete inversion after radical attack (Fig. 6) because of the partial loss of methylene groups connected with the formation of CH_3SH and the structural changes connected to the decarboxylation reaction. Differently, in the presence of oxygen, the desulfurisation reaction is expected to give rise to the mutation of Met into HomoSer (Scheme 1) [14]. The IR measurements were able to detect also this degradation product. In fact, only in the N_2O/O_2 experiment, a new broad band due to νO–H mode was visible in the IR spectrum at about 3,420 cm^{-1} (Fig. 5A (c)). By using the difference spectrum, this spectral change was even more evident (Fig. 5B (b)).

Significant intensity changes were visible both in the COO^- and NH_3^+ bands in the IR and Raman spectra (Figs. 5, 6, and 7), as observed in N_2O-saturated solutions,

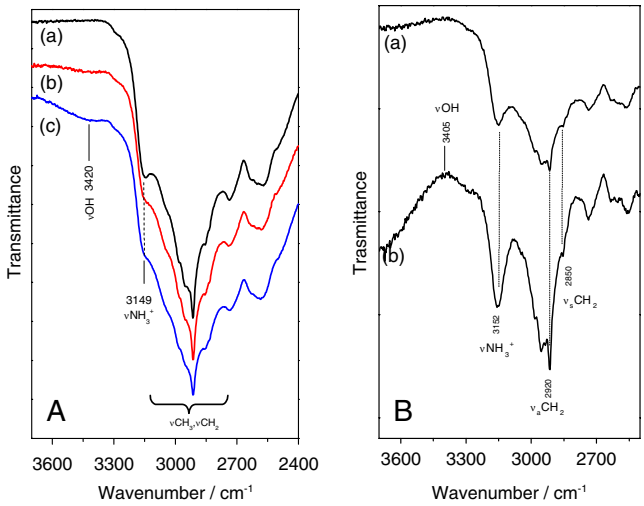

Fig. 5 **A** The 3,700–2,400-cm^{-1} IR region of Met (**a**) before and after 4 kGy irradiation under N_2O (**b**) or N_2O/O_2 (90/10) (**c**) saturation. **B** Difference spectra obtained by subtracting the IR spectrum of irradiated Met under N_2O (**a**) or N_2O/O_2 (**b**) from that of untreated Met

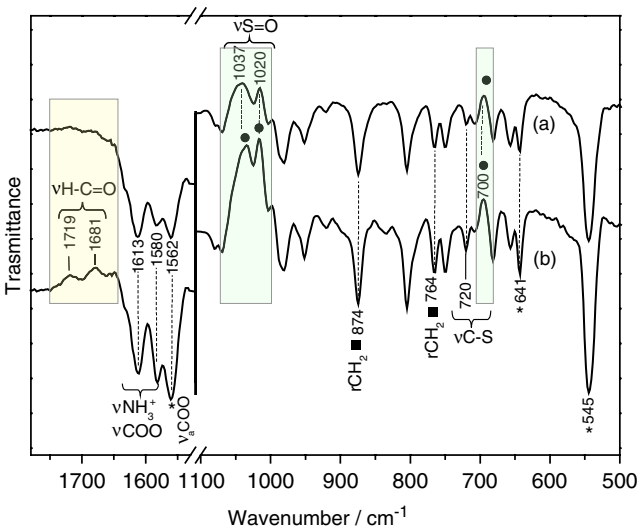

Fig. 7 The 1,800–500-cm^{-1} IR region of the difference spectra obtained by subtracting the spectrum of Met irradiated under N_2O (**a**) or N_2O/O_2 (90/10) (**b**) saturation from untreated Met. The bands due to the formation of degradation products are evidenced by the *light yellow* and *green* area. *Asterisks* and *circles* marker bands of changes involving COO^- and the sulfur-containing moiety, respectively

and are compatible with the decarboxylation and deamination reactions expected to occur as a consequence of the ·OH radical attack on Met (Scheme 1). Differently, in the presence of oxygen, a new weak IR band at about 1,715 cm^{-1} was visible (Fig. 4). By using the difference spectrum to stress this small spectral change, two weak bands at 1,719 and 1,681 cm^{-1} were evidenced (Fig. 7b). These absorptions can be connected with the formation of aldehyde groups, since they are attributable to the stretching mode of free and H-bonded–HC = O moieties [38], in agreement with the expected formation of MTPA (Scheme 1). Aldehyde groups are known to be formed also in the absence of O_2, although in a much lesser amount, but the weakness of the corresponding IR band does not allow the undoubted assignment.

The Raman and IR spectra of the irradiated sample show the chemical species which contribute significantly to the spectrum profile are Met(O) (~1,040 and 700 cm^{-1}, Raman and IR), HomoSer (3,420 cm^{-1}, IR) and MTPA (~1,720 and 1,680 cm^{-1}, IR).

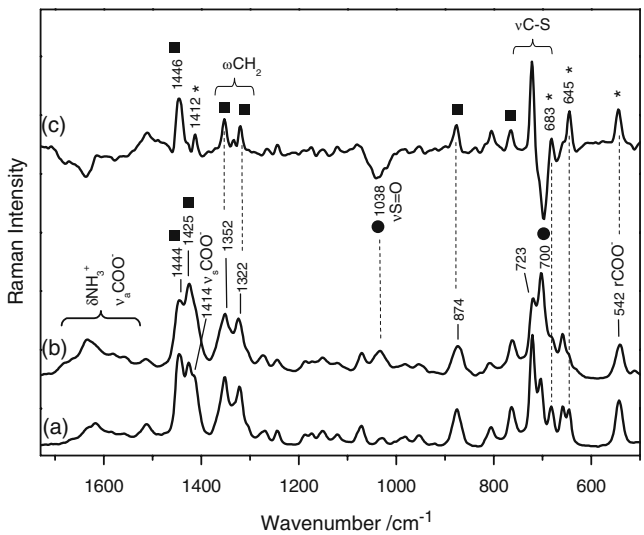

Fig. 6 The 1,750–500-cm^{-1} Raman region of Met (**a**) before and after 4 kGy irradiation under N_2O/O_2 (90/10) (**b**) saturation; **c** difference spectrum obtained by subtracting the spectrum of Met irradiated (N_2O/O_2, 90/10) from untreated Met (**a**–**b**). *Asterisks*, *squares* and *circles* marker bands of changes involving COO^-, CH_2/CH_3 and S-containing moieties, respectively

Conclusions

Data included in this work highlight the potential of Raman and IR spectroscopy to be used, in combination with other analytical strategies, for monitoring the formation of degradation products of amino acids like Met after radical stress exposure. In fact, both the Raman and IR spectra present some marker bands useful for the identification of the main degradation mechanisms and of some products formed. On one hand, Raman spectroscopy is a useful tool for revealing the occurrence of decarboxylation reactions and radical-based modifications in the sulfur-containing moiety of Met, since both the formation of the main oxidation product (Met(O)) and the loss of methylene moiety, due to the desulfurisation process, are visible. On the other hand, the IR spectra allow to detect processes like deamination and decarboxylation, as well as the formation of degradation products such as MTPA, HomoSer and Met(O).

These information combine to produce a set of spectroscopic markers of the main processes occurring as a consequence of radical stress exposure which can be used in a spectroscopic protocol for providing a first characterisation for the degradation processes also in more complex systems such as peptides and proteins.

Acknowledgements The support and sponsorship concerned by CNR-CONICET joint research project 2009–2010 and COST Action CM0603 on "Free Radicals in Chemical Biology (CHEMBIORADICAL)" are kindly acknowledged.

References

1. Vogt W (1995) Free Rad Biol Med 18:93–105
2. Stadtman ER, Moskovitz J, Levine RL (2003) Antiox Redox Signal 5:577–582
3. Koteliansky VE, Domogatsky SP, Gudkov AT (1978) Eur J Biochem 90:319–323
4. Brot N, Weissbach H (1983) Arch Biochem Biophys 223:271–281
5. Johnson D, Travis J (1979) J BiolChem 254:4022–4026
6. Wang WR, Vlasak J, Li YS, Pristatsky P, Fang YL, Pittman T, Roman J, Wang Y, Prueksaritanont T, Ionescu R (2011) Mol Immunol 48:860–866
7. Snijder J, Rose RJ, Raijmakers R, Heck AJR (2010) J Struct Biol 174:187–195
8. Levine RL, Mosoni L, Berlett BS, Stadtman ER (1996) PNAS 93:15036–15040
9. Reddy VY, Desrochers PE, Pizzo SV, Gonias SL, Sahakian JA, Levine RL, Weiss SJ (1994) J Biol Chem 269:4683–4691
10. Davies MJ (2005) Biochim Biophys Acta-Proteins and Proteomics 1703:93–109
11. Hawkins CL, Davies MJ (2001) Biochim Biophys Acta-Bioenerg 1504:196–219
12. Davies MJ, Fu SL, Wang HJ, Dean RT (1999) Free Rad Biol Med 27:1151–1163
13. Schoneich C (2005) Biochim Biophys Acta -Protein Proteomics 1703:111–119
14. Barata-Vallejo S, Ferreri C, Postigo A, Chatgilialoglu C (2010) Res Toxicol 23:258–263
15. Hawkins CL, Morgan PE, Davies MJ (2009) Free Rad Biol Med 46:965–988
16. Salzano AM, Renzone G, Scaloni A, Torreggiani A, Ferreri C, Chatgilialoglu C (2011) Mol Biosyst 7:889–898
17. Ferreri C, Chatgilialoglu C, Torreggiani A, Salzamo AM, Renzone G, Scaloni A (2008) J Proteome Res 7:2007–2015
18. Chatgilialoglu C, Ferreri C, Torreggiani A, Salzano AM, Renzone G, Scaloni A (2011) J Proteomics. doi:10.1016/j.jprot.2011.03.012
19. Spinks JWT, Woods RJ (1990) An introduction to radiation chemistry, 3rd edn. Wiley, New York, p 100
20. Buxton GV, Greenstock CL, Helman WP, Ross AB (1988) J Phys Chem Ref Data 17:513–886
21. Ross ABMW, Helman WP, Buxton GV, Huie RE, Neta P (eds) (1998) NDRL-NIST solution kinetic database-version 3. Notre Dame Radiation Laboratory, Notre Dame
22. Garrison WM (1987) Chem Rev 87:381–398
23. Winterbourn CC (1995) Toxicol Lett 82–3:969–974
24. Steinberg D, Witztum JL (2002) Circulation 106:E195
25. Piraud M, Vianey-Saban C, Petritis K, Elfakir C, Steghens JP, Morla A, Bouchu D (2003) Rapid Commun Mass Spectrom 17:1297–1311
26. Ravi J, Hills AE, Cerasoli E, Rakowska PD, Ryadnov MG (2011) Eur Biophys J 40:339–345
27. Lord RC, Yu N-t (1970) J Mol Biol 50:509–524
28. Mary MB, Umadevi M, Pandiarajan S, Ramakrishnan V (2004) Spectrochim Acta Part a-Mol Biomol Spectrosc 60:2643–2651
29. Lima JA, Freire PTC, Melo FEA, Lemos V, Mendes J, Pizani PS (2008) J Raman Spectrosc 39:1356–1363
30. Torreggiani A, Tamba M, Ferreri C (2007) Prot Pept Letters 14:716–722
31. Torreggiani A, Tamba M, Manco I, Faraone-Mennella MR, Ferreri C, Chatgilialoglu C (2006) Biopolymers 81:39–50
32. Torreggiani A, Domenech J, Orihuela R, Ferreri C, Atrian S, Capdevila M, Chatgilialoglu C (2009) Chem Eur J 15:6015–6024
33. Ferreri C, Manco I, Faraone-Mennella MR, Torreggiani A, Tamba M, Manara S, Chatgilialoglu C (2006) ChemBioChem 7:1738–1744
34. Jurasekova Z, Tinti A, Torreggiani A (2011) Anal Bioanal Chem 400:2921–2931
35. Rajkumar BJM, Ramakrishnan V (2001) Spectrochim. Acta, Part A, Mol Biomol Spectrosc 57(2):247–254
36. Koleva BB (2007) Vibr Spectrosc 44:30–35
37. Grunenberg A, Bougeard D (1987) J Mol Struct 160:27–36
38. Colthup NB, Daly LH, Wiberley SE (1990) Introduction to infrared and raman spectroscopy. Academic, New York